Applied Catalysis B: Environmental 162 (2015) 11–20

Contents lists available at ScienceDirect

Applied Catalysis B: Environmental

journal homepage: www.elsevier.com/locate/apcatb

Rational preparation of Ag and Au bimetallic catalysts for the hydrocarbon-SCR of NO_x: Sequential deposition vs. coprecipitation method

P.M. More[a,b], D.L. Nguyen[d], M.K. Dongare[a,c], S.B. Umbarkar[a,b,1], N. Nuns[d], J.-S. Girardon[d], C. Dujardin[d], C. Lancelot[d], A.-S. Mamede[d], P. Granger[d,*]

[a] National Chemical Laboratory, Dr. Homi Bhabha Road, Pashan, Pune 411008, India
[b] Academy of Scientific and Innovative Research, CSIR, Anusandhan Bhawan, New Delhi 110 001, India
[c] Mojj Engineering Systems Ltd, 15-81/B, MIDC, Bhosari, Pune 411026, India
[d] Unité de Catalyse et de Chimie du Solide, UMR CNRS 8181, Université Lille1, Sciences et Technologies, Cité Scientifique, Bâtiment C3, 59655 Villeneuve d'Ascq Cedex, France

ARTICLE INFO

Article history:
Received 22 April 2014
Received in revised form 17 June 2014
Accepted 19 June 2014
Available online 26 June 2014

Keywords:
HC-SCR
Au–Ag particles
Co-precipitation
DeNO$_x$ reaction

ABSTRACT

This study emphasizes the importance of the preparation method for bimetallic Au–Ag catalysts supported on alumina in the selective reduction of NO_x by hydrocarbons with gas feed compositions representative of diesel fuelled engine exhaust gas. An optimal balance between oxidative and reductive surface properties is obtained when Au and Ag are successively introduced. Significant re-dispersion processes take place when the catalyst runs at 500 °C leading to a gain in activity at low temperature and ascribed to a better interaction between Au and Ag species. Co-precipitation leads to a preferential formation of intermetallic Au–Ag particles which is detrimental to the catalytic performances. Aging at 500 °C leads to a significant particle sintering and a strengthening of the metallic character.

1. Introduction

Actually, commercial Lean-NO_x Trap (LNT) [1] and urea-Selective Catalytic Reduction (SCR) technologies are widespread [2] but still suffer from significant drawbacks due to the implementation of complex architectures including urea injection systems and the use of precious metal catalysts to pre-oxidize NO, activate the fast SCR process or store NO_x on LNT systems. Strong kinetic and thermodynamic limitations are generally associated with both technologies which lead to narrower operating windows. Further optimization of complex dosage strategies for urea injection [3] is an important outcome to avoid deactivation phenomena [4]. Tentative developments combining both technologies [5] as well as optimizing dual-layer (SCR + LNT) systems [6] are promising but not enough mature to envision rapid commercial applications. In this context, the selective reduction of NO_x using unburnt hydrocarbons still remains an attractive solution because the use of platinum group metal (PGM) based catalysts in this technology is not a prerequisite. Indeed, gold and silver can be considered as potential substitutes for PGM in end-of-pipe technologies for diesel engines enhancing significantly the selective conversion of NO_x to nitrogen in a wider operating window [7–11]. Earlier investigations, reported broad and high conversion ranges at moderate temperature on Ag/Al_2O_3 [12,13] whereas gold seems to be more active at higher temperature [7]. Previous attempts led to significant rate enhancement at low temperature when gold interacts with Mn_2O_3 [14]. In most cases, a bi-functional catalysis involving metallic and oxidic sites to oxidize NO to NO_2 and to activate the SCR reaction, respectively, is currently envisioned. Hence, one of the objectives of this study was to combine both Au and Ag to promote synergistic effects then obtaining a complete selective conversion of NO to N_2 at lower temperatures and a broader operating window compared to single Ag and Au based catalysts.

In a recent paper, Hamill et al. showed that the combination of gold and palladium leads to a strong synergistic effect compared to the catalytic properties of the individual metals [15]. Alloying gold with PGM can be useful for exhaust gas treatment systems running at high temperature then limiting the detrimental effects due to particle sintering especially under wet atmosphere. Indeed, noble metals exhibiting higher melting points can slower gold particle

* Corresponding author. Tel.: +33 320 434 938; fax: +33 320 436 561.
E-mail addresses: sb.umbarkar@ncl.res.in (S.B. Umbarkar), Pascal.granger@univ-lille1.fr (P. Granger).
[1] Tel.: +91 2025 902 044.

http://dx.doi.org/10.1016/j.apcatb.2014.06.031
0926-3373/

Table 1
Elemental composition and textural properties of bimetallic gold–silver catalysts supported on alumina.

Catalyst	Preparation method		Bulk composition (wt.%)		Textural properties	(N_2 physisorption)	
			Ag	Au	S_{BET} ($m^2\ g^{-1}$)	d_P (nm)	V_P ($cm^3\ g^{-1}$)
Al_2O_3			–	–	450	6.1	1.10
Ag/AuAl	Sequential deposition	Fresh	1.04	0.80	224	7.8	0.51
		Aged			216	7.8	0.52
Au/AgAl	Sequential deposition	Fresh	1.01	0.60	281	3.6	0.34
		Aged			229	4.4	0.35
Au–Ag/Al	Co-precipitation	Fresh	0.98	0.90	224	8.0	0.61
		Aged			207	9.1	0.56

sintering when they are alloyed [16,17]. Different types of interactions can exist when Au interacts with metallic substrates, such as Ag especially with oxidic silver species which can act as spacer preventing the aggregation of gold particles [18]. As a matter of fact, the optimization of bimetallic Ag–Au catalysts is not an easy task and usually needs a better understanding of the physical origin of synergy currently ascribed to geometric or electronic effects due to the highest electronegativity of gold among the transition metals. Based on these considerations, the methodology selected for the preparation of bimetallic Au–Ag catalysts (impregnation, co-precipitation, thermal treatment . . .) may drastically affect their catalytic properties. By way of illustration, high activity and stability in CO oxidation for Au–Ag/TiO_2 catalyst prepared by sequential deposition-precipitation was ascribed to a compromise between metal particle size and the bimetallic character of the particles [19,20]. However, some discrepancies sometimes arise. It is particularly true for the low temperature CO oxidation performed on gold–silver alloy formed during one pot synthesis of the bimetallic catalyst for which 20–30 nm large particles exhibit an exceptionally high activity for CO conversion to CO_2 [21]. Such a result differs from previous statements demonstrating that nano sized gold particles below 5 nm are generally intrinsically more active.

Based on these previous observations, in this study we have compared two different methods for the preparation of bimetallic Au–Ag supported on alumina for the selective catalytic reduction of NO_x in lean burn conditions which can originate different types of interactions between Au and Ag segregated on alumina or alloyed in bimetallic particles. It was found that co-precipitation and two-step deposition routes lead to drastic changes in their catalytic performances. Such differences have been tentatively rationalized on the basis of extensive bulk and surface characterizations.

2. Experimental

2.1. Catalyst synthesis

2.1.1. Sequential deposition method

Initially 1 wt.% Au/Al_2O_3 was prepared by deposition-precipitation method using urea. $HAuCl_4$ solution was dropwise added to a slurry of γ-alumina in water at 80 °C with constant stirring. Urea solution was added dropwise to the above solution in order to promote the precipitation of $Au(OH)_3$ on the surface of alumina. The solid thus obtained was filtered and abundantly washed with water to remove chloride until the lack of silver chloride precipitation after addition of aqueous solution of $AgNO_3$ in the waste water. The solids were subsequently dried at 80 °C for 12 h. Afterwards, the gold loaded catalyst (Au/Al_2O_3) was impregnated with an aqueous $AgNO_3$ solution with adjusted concentration in order to get 1 wt.% Ag in Ag-Au/Al_2O_3 catalyst. For Au–Ag/Al_2O_3, the starting material was 1 wt.% Ag/Al_2O_3 prepared by impregnation on γ-alumina by an aqueous $AgNO_3$ solution according to the same experimental conditions. After drying at 80 °C for 12 h, gold was added via the above-mentioned deposition-precipitation method. The obtained sample was filtered and washed with water till complete removal of chloride. Each sample was finally dried at 80 °C for 12 h and then calcined in air at 500 °C for 6 h. The bimetallic Au–Ag/Al_2O_3 and Ag–Au/Al_2O_3 were labelled as Au/AgAl and Ag/AuAl, respectively.

2.1.2. Coprecipitation

Au–Ag/Al_2O_3 was prepared by simultaneous co-precipitation of aqueous solutions of $HAuCl_4$ and $AgNO_3$ added to a slurry of γ-alumina in water maintained at a constant temperature of 80 °C with constant stirring. The precipitation of gold and silver as hydroxides precursors was obtained by adding dropwise urea solution. The slurry was dried at 80 °C for 12 h and calcined at 500 °C for 6 h and labelled Au–Ag/Al.

2.2. Physicochemical characterization

2.2.1. Bulk characterization

X-ray powder diffraction patterns were collected on a Philips (X pert) diffractometer equipped with a Ni filtered Cu $K\alpha$ radiation (λ = 1.5406 Å, 40 kV, 30 mA). The data were collected in the 2θ range 30–90° with a step of 0.02° and scan rate of 4° min^{-1}. UV–visible DRS spectra were recorded with a UV–visible spectrophotometer (Perkin Elmer, Lambda 650) in the diffuse reflectance mode between 200 and 800 nm at a step of 0.2 nm with a slit width of 1 nm. $BaSO_4$ was used as reference sample. TEM measurements were performed with Tecnai FEI G2 microscope, using an accelerating voltage of 200 kV and a LaB6 mono-crystal. For TEM analysis, all samples were deposited on a carbon coated 200 mesh Cu grid. Gold and silver were analysed by inductively coupled plasma atomic emission spectroscopy (ICP-AES) at the chemical analysis centre of the CNRS. Elemental analysis data are collected in Table 1. It was found that chlorine content was lower than 2000 ppm in all calcined samples.

2.2.2. Surface characterization

The specific surface area of the calcined samples was determined by N_2 sorption at −196 °C using NOVA 1200 (Quanta Chrome) equipment. Prior to N_2 physisorption, the sample was outgassed at 300 °C under vacuum. The specific surface area, S_{BET}, was calculated according to the BET equation and the pore size distribution from the nitrogen adsorption isotherm by using the BJH (Barrett–Joyner–Halenda) method. XPS experiments were performed on an AXIS Ultra^{DLD} Kratos spectrometer equipped with a monochromatized aluminium source for excitation (150 W). The analyzer was operated in a constant pass energy mode (E_{pass} = 40 eV). The Al 2p (74.6 eV) binding energy (BE) from Al_2O_3 was used as internal reference. Peak area was estimated after subtracting the background according to the procedure suggested by Shirley [22]. Time-of-flight secondary ion mass spectrometry

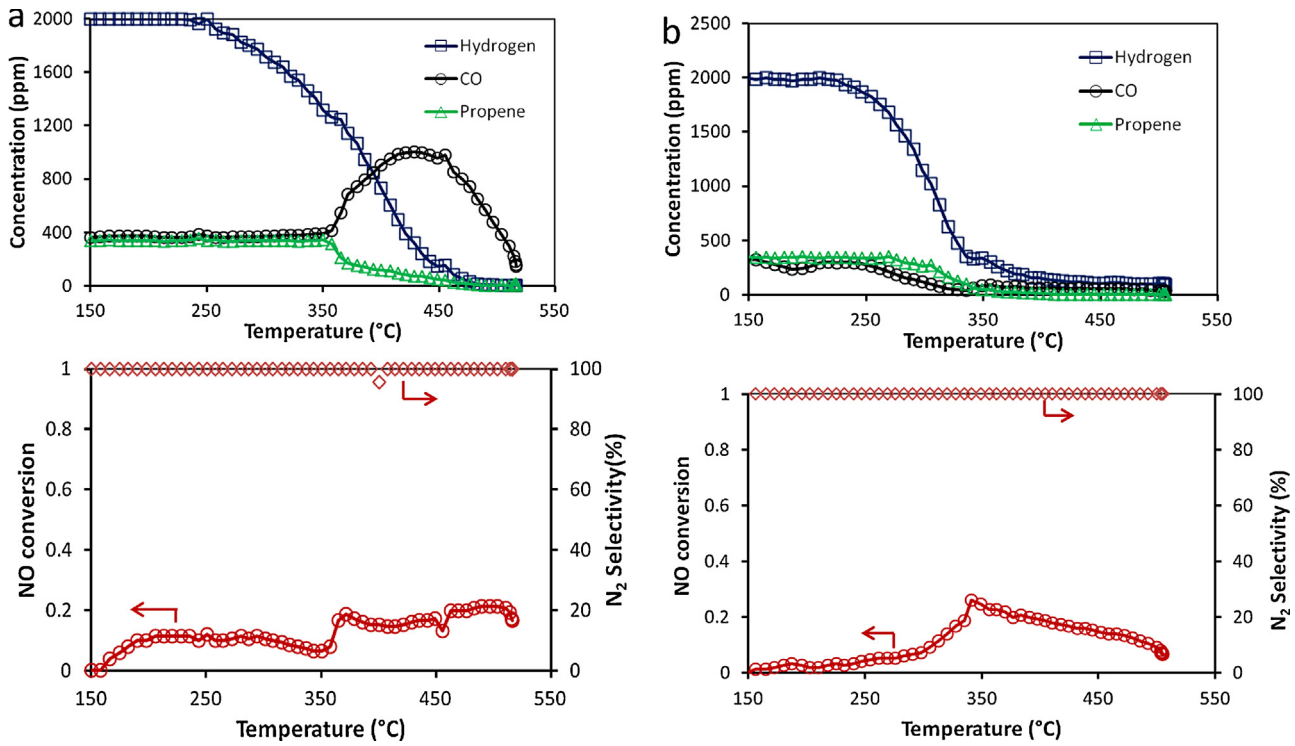

Fig. 1. Comparison of NO_x SCR performances on co-impregnated Au–Ag/Al sample pre-reduced in H_2 at 250 °C from TPR-1 experiment (a) and on aged sample after exposure overnight in reaction conditions at 500 °C from TPR-2 (b). Reaction feed: 300 ppm NO, 300 ppm CO, 300 ppm C_3H_6, 2000 ppm H_2, 100 ppm $C_{10}H_{22}$, 10 vol.% O_2, 10 vol.% CO_2, 5 vol.% H_2O, He balance. GHSV: 50,000 h^{-1}.

(ToF-SIMS) and low energy ion scattering (LEIS) were utilized for analyzing the composition of the outermost surface of materials under ultra-high-vacuum (UHV) conditions. Practically, primary Bi_3^+ ion doses (25 keV and 0.25 pA current) are pulsed at the surface of the catalysts during the ToF-SIMS measurements (TOF SIMS V, ION TOF GmbH). Low Energy Ion Scattering measurements were performed on a Qtac^{100} spectrometer (ION TOF GmbH) as earlier described [23]. LEIS measurements were performed with 3 keV $^4He^+$ scattering. A sputter yield of 0.2 atoms per He-ion was assumed with a primary beam current of 4 nA and an analysed area of 500 μm × 500 μm.

2.3. Catalytic measurements

Temperature-programmed reaction (TPR) experiments were performed in a fixed bed flow reactor by using 300 mg of catalyst exposed to a gas mixture composed of 300 ppm NO, 300 ppm CO, 300 ppm C_3H_6, 2000 ppm H_2, 100 ppm $C_{10}H_{22}$, 10 vol.% O_2, 10 vol.% CO_2, 5 vol.% H_2O and He balance. The total flow rate was adjusted to 300 mL min^{-1} in order to get a gaseous hourly space velocity of 50,000 h^{-1}. Reactants and products were analysed on-line by using a CP4900 Varian micro-GC which allowed the separation and the quantification of CO, H_2, nitrogen, propene and N_2O. Specific MIR9000 NO_x analyzer supplied by Environment SA were utilized for measuring the specific response of NO and NO_2.

Prior to reaction, the catalyst samples were pre-reduced in pure H_2 at 250 °C. After a first TPR-1, with a heating rate $dT/dt = 2$ °C min^{-1}, in the above-mentioned specific operating conditions the catalyst samples were kept in isothermal conditions at 500 °C overnight under reaction feed. After cooling down at 80 °C, a second TPR-2 was performed in similar experimental conditions. The NO conversion (X_{NO}) was calculated from outlet molar flow rates of N_2 and N_2O, respectively, F_{N_2}, F_{N_2O} and inlet molar flow rate of NO ($F_{NO,0}$) according to Eq. (1). The selectivity towards nitrogen formation S_{N_2} was given by Eq. (2).

$$X_{NO} = \frac{2 \times \left(F_{N_2} + F_{N_2O}\right)}{F_{NO,0}} \quad (1)$$

$$S_{N_2} = \frac{F_{N_2}}{F_{N_2} + F_{N_2O}} \quad (2)$$

3. Results and discussion

The influence of the preparation method (sequential deposition vs. coimpregnation) for the elaboration of supported bimetallic gold–silver catalysts will be discussed based on the comparison of their catalytic properties and changes in structural and surface properties on fresh and aged catalysts after reaction at 500 °C. As 2 wt.% Ag/Al_2O_3 [13] and 2 wt.% Au/Al_2O_3 (see Ref. [7]) have shown promising activity for HC-SCR, we kept constant the metal loading on all bimetallic catalysts i.e. 2 wt.%. Consequently, 1 wt.% Ag and 1 wt.% Au were loaded on alumina. First, it has been shown that different types of interactions between Au and Ag can be created according to the preparation route which drastically influences their performance and can lead to different surface reconstruction under reaction conditions.

3.1. Catalytic properties of bimetallic Ag–Au catalysts in the hydrocarbon-SCR of NO_x

3.1.1. Au–Ag/Al_2O_3 catalyst prepared by coprecipitation

Prior to catalytic measurements, all samples were pre-reduced in pure H_2 at 250 °C. Temperature-programmed NO conversion curves are collected in Fig. 1(a) showing a poor activity with maximum NO conversion lower than 23% in the whole temperature range on the pre-reduced sample. Only nitrogen is produced with no significant gaseous N_2O and NO_2 formation. As seen the

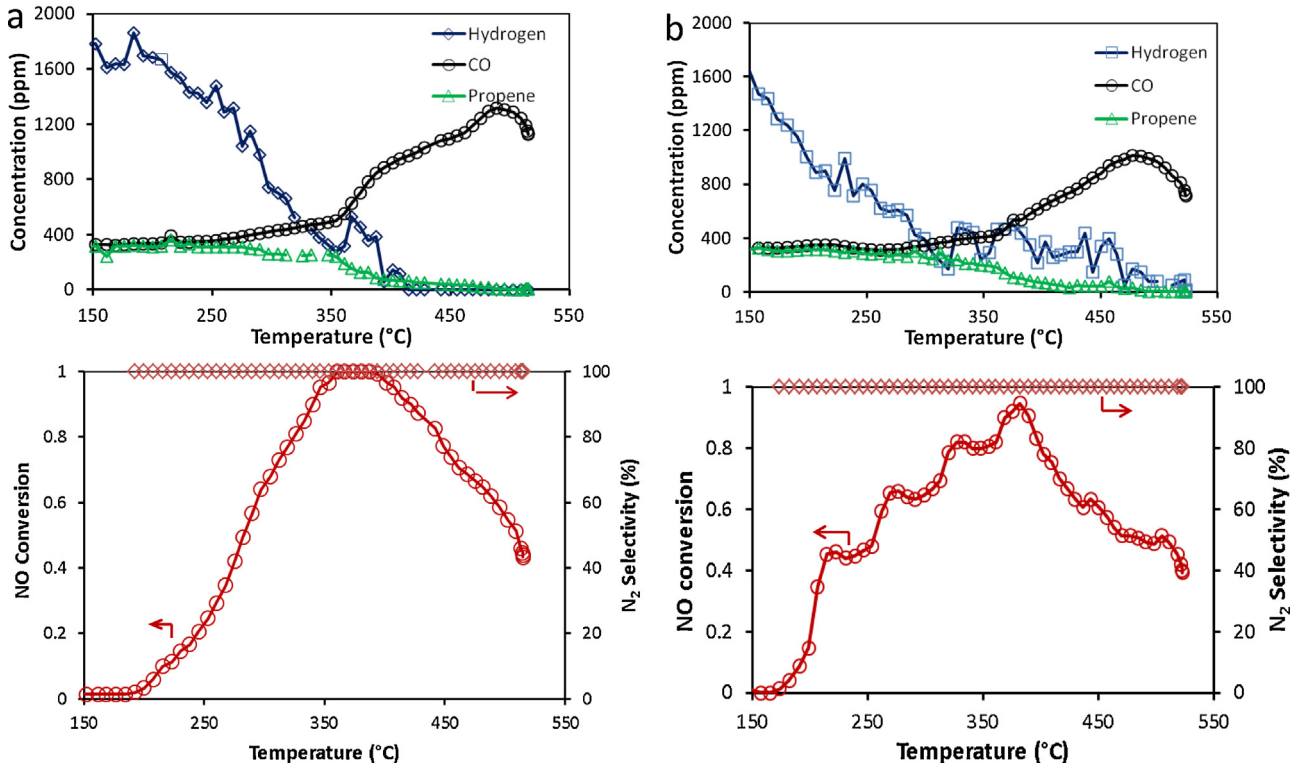

Fig. 2. Comparison of NO_x SCR performances on impregnated Ag/AuAl sample pre-reduced in H_2 at 250 °C from TPR-1 experiment (a) and on aged sample after exposure overnight in reaction conditions at 500 °C from TPR-2 (b). Reaction feed: 300 ppm NO, 300 ppm CO, 300 ppm C_3H_6, 2000 ppm H_2, 100 ppm $C_{10}H_{22}$, 10 vol.% O_2, 10 vol.% CO_2, 5 vol.% H_2O, He balance. GHSV: 50,000 h^{-1}.

concentration of H_2 gradually decreases above 200 °C with a complete conversion at 450 °C. Regarding propene, the concentration remains unchanged up to ~350 °C then a discontinuity appears coinciding with a parallel conversion of NO and CO formation. These results agree with previous observations on gold [7] and silver based catalysts [24] showing that the direct reduction of NO by hydrogen should not occur. The extra formation of CO has been previously explained by the involvement of reforming and/or partial

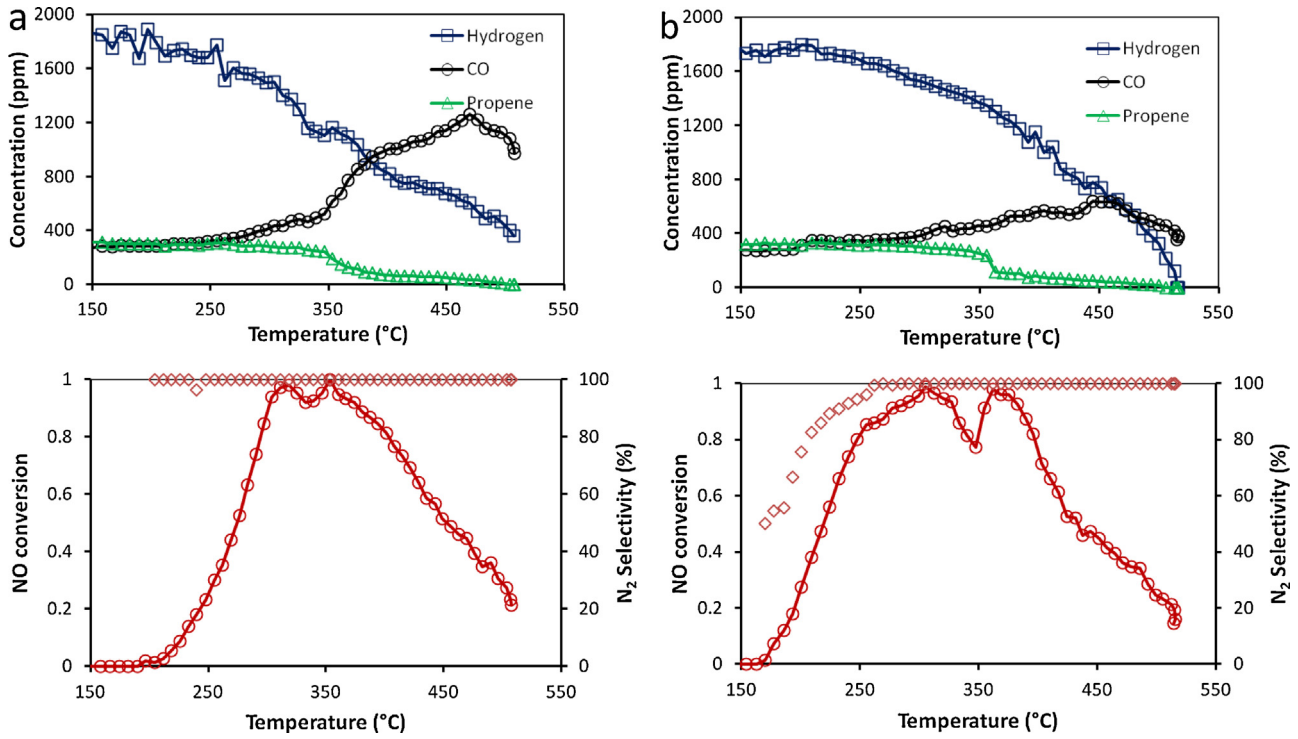

Fig. 3. Comparison of NO_x SCR performances on co-impregnated Au/AgAl sample pre-reduced in H_2 at 250 °C from TPR-1 experiment (a) and on aged sample after exposure overnight in reaction conditions at 500 °C from TPR-2 (b). Reaction feed: 300 ppm NO, 300 ppm CO, 300 ppm C_3H_6, 2000 ppm H_2, 100 ppm $C_{10}H_{22}$, 10 vol.% O_2, 10 vol.% CO_2, 5 vol.% H_2O, He balance. GHSV: 50,000 h^{-1}.

oxidation of decane [7,12]. In the presence of water, the residual concentration of H_2 and CO is also governed by the water–gas-shift reaction. While we cannot exclude that NO can be partly reduced by propene, it was found that decane plays a crucial role. Indeed, the absence of decane in the feed induces a quasi-complete suppression of NO conversion especially at low temperature [7,12]. TPR-2 experiments illustrated in Fig. 1(b) do not reveal significant improvement in NO conversion. On the contrary, NO conversion in the low temperature range attenuates. The most prominent observation is related to the lack of extra CO production likely due a significant rate enhancement of CO, H_2 and propene oxidation into CO_2 and H_2O suggesting that the balance between the reductive and oxidative properties of the catalyst have been modified after exposure to the reaction mixture overnight at 500 °C.

3.1.2. *Au–Ag/Al_2O_3 catalysts prepared by sequential deposition*

Two different samples were prepared starting from Au/Al_2O_3 prepared by deposition-precipitation then impregnated with aqueous solution of silver nitrate (Ag/AuAl) or impregnated Ag/Al_2O_3 sample where gold was subsequently incorporated by deposition–precipitation (Au/AgAl). Similarly, both were pre-reduced in H_2 at 250 °C. Their catalytic performances are presented in Figs. 2 and 3. As seen, significant improvements are observed in NO conversion compared to co-precipitated samples. A typical volcano-type NO conversion curve is observed which highlights the role of NO_2 as key intermediate in the overall process of the selective reduction of NO_x. This behaviour has been initially described over noble metals [25] and silver based catalysts [26]. NO dissociation on the metallic particles is not a major route in the overall reduction process under lean conditions (in an excess of oxygen). Burch et al. [25] proposed that it can go through spill-over of NO_2 from the metal to the support to react with C_xH_y ad-species stored on the support. Hence, this typical volcano-type curve is generally explained by NO conversion to NO_2 kinetically limited at low temperature and thermodynamically unfavoured at high temperature. As seen on the pre-reduced sample from TPR-1, a quasi-complete NO conversion to nitrogen is achieved on Ag/AuAl in the range 180–420 °C (see Fig. 2a). On the aged catalyst, TPR-2 in Fig. 2b reveals a slightly lower maximum conversion at 95%. More importantly, a broadening of the operating window with significant enhancement in NO conversion to N_2 at low temperature is observed. Interestingly, it is remarkable that the conversion profiles for CO, propene and H_2 remain quasi-unchanged compared to previous observations on the co-precipitated sample. Hence, after exposure overnight at 500 °C under reaction mixture, Ag/AuAl remains stable preserving a good compromise between its oxidative and reductive properties. This is also true for Au/AgAl with a more extensive conversion of NO at low temperature with 100% selectivity to nitrogen formation (Fig. 3). After exposure overnight at 500 °C, TPR-2 reveals the same tendency as previously described with a broadening of the operating window and a slight detrimental effect on the selectivity behaviour highlighted by a significant formation of N_2O below 230 °C (Fig. 3b).

3.2. *Comparative bulk and surface properties of freshly-pretreated and aged supported Au–Ag/Al_2O_3 catalysts*

3.2.1. *Characterization of different types of interactions between gold and silver according to the preparation protocol*

XRD patterns recorded on bimetallic $Au–Ag/Al_2O_3$ are collected in Fig. S1 (Supplementary Materials). Similar lines appear in all diffractograms at 2θ—38.2°, 44.5°, 77.5° ascribed to the (1 1 1), (2 0 0) and (2 2 0) planes characteristic of Ag, Au and Au–Ag solid solution in agreement with earlier investigations [27–29]. UV–visible spectroscopic measurements provide different spectral features on samples prepared by sequential deposition and co-precipitation. Preliminary experiments collected in Fig. 4 on single Au/Al_2O_3 catalysts revealed the characteristic excitation of surface plasmon resonance of metallic gold particles at 550 nm [30,31]. For Ag/Al_2O_3, absorption bands arise at 222, 257, 292 and 346 nm previously ascribed to a $4d^{10} \rightarrow 4d^9s^1$ transition characteristic of highly dispersed Ag^+ ions and small $Ag_n^{\delta+}$ clusters, respectively [32]. Fig. 5 shows UV–visible spectra recorded on bimetallic Au–Ag samples. As shown, significant shifts are distinguishable on the 550 nm absorption band previously ascribed to gold nano-particles compared to the reference monometallic gold catalyst. Parallel, to these observations, spectra recorded on bimetallic samples prepared by sequential deposition are mainly characterized by UV–visible bands previously ascribed to Ag^+ ions and/or small $Ag_n^{\delta+}$. No significant contribution in the range 300–450 nm related to the excitation of large metallic Ag particles is discernible as reported elsewhere on bimetallic Au/Ag composite film [33]. Based on these observations, the characterization of Ag^+ and/or $Ag_n^{\delta+}$ species as well as gold metallic species on Au/AgAl and Ag/AuAl would suggest a preferential segregation of Au and Ag rather than the formation of alloyed Au–Ag particles. On the contrary, the presence of only one contribution on Au–Ag/Al displaying a red shift (522 nm) compared to single gold catalyst has

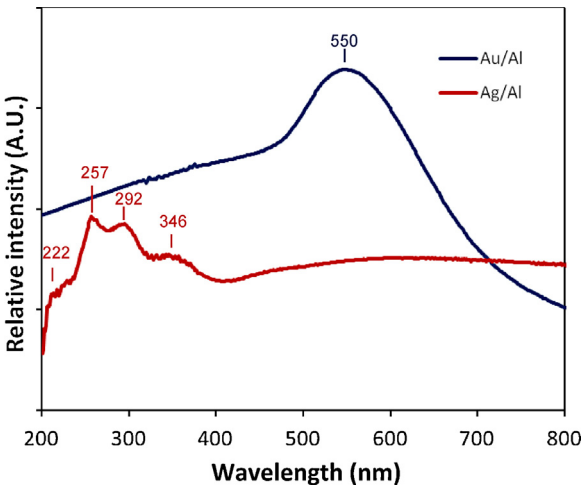

Fig. 4. UV–visible DRS spectra recorded on freshly-prepared (a) Au/Al_2O_3 (Au/Al) and on (b) Ag/Al_2O_3 (Ag/Al).

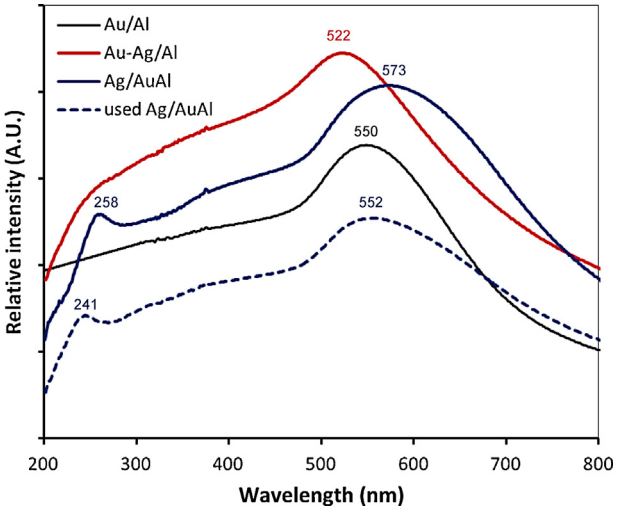

Fig. 5. UV–visible DRS spectra recorded on freshly-prepared bimetallic Au–Ag catalysts supported on alumina prepared by co-precipitation Au–Ag/Al, sequential deposition Au/AgAl and on aged Au/AgAl.

been earlier discussed and tentatively assigned to the formation of alloyed and/or intermetallic Au–Al particles [28]. Hence, based on those observations, it can be suggested that segregated cationic and metallic Au and Ag species would coexist in the samples prepared by sequential deposition while only single or intermetallic Au–Ag particles would predominate on the co-precipitated sample.

Surface analysis combining XPS, LEIS and ToF-SIMS analysis provides more arguments which converge to the preferential segregation of Au and Ag and/or weakly interacting on Au/AgAl and Ag/AuAl whereas bimetallic particles would preferentially form on Au–Ag/Al. XPS spectral features are summarized in Table 2. Particular attention was paid to the characteristic Au $4f_{7/2}$ and Ag $3d_{5/2}$ photopeaks of gold and silver, respectively. B.E. values in Table 2 are consistent with gold in metallic state [28,33]. For silver, B.E. values mostly reflect the presence of metallic species but no decisive conclusions can be drawn regarding the presence of cationic Ag species. In fact, more precise information regarding the oxidation state of silver would be obtained by examining the peak kinetic energy of the Auger MNN transition line recognized as more sensitive to the chemical environment than the corresponding XPS Ag 3d photopeak [34,35]. Semi-quantitative analysis reveals a sharp silver enrichment on samples prepared by sequential deposition whereas the surface composition doesn't differ from the bulk one for the co-precipitated catalyst taking into account the relative accuracy.

ToF-SIMS is a useful technique to analyse the outermost layers of catalysts. Practically, primary Bi_3^+ ions were pulsed at the surface of the samples representing 10^{12} ion doses per cm^2. In these static conditions, less than 1% of the analysed depth (1–3 nm) is sputtered during the analysis. After bombardment, secondary ions are emitted and can be analysed with different polarities leading to the detection of positive or negative fragments which can reflect the local chemical environment of surface atoms. The different fragments *i* analysed with their relative abundance corresponding to the intensity I_i of the fragment *i* to the global intensity of all fragments $I_i/\Sigma I_i$ are collected in Table 3. As seen, the presence of trace amount of chlorine is detected preferentially bonded to silver. Particular attention was paid to specific fragments combining Ag and Au since they would evidence the presence of intermetallic compounds [36]. Interestingly, Fig. 6 underlines that the most abundant Ag_2Au^+ is only detected on bimetallic Ag–Au/Al prepared by co-precipitation whereas the lack of observation of this fragment suggests the absence of significant formation of bimetallic particles on Ag/AuAl samples prepared by sequential deposition. More information can be obtained from LEIS which is an analytical tool that provides information on the atomic composition of the first atomic layer. Fig. 7 shows a typical LEIS spectrum of the co-impregnated Au–Ag/Al catalyst after a sputtered depth of around 1.5 monolayers. As exemplified four peaks are clearly distinguishable at 1192 eV, 1726 eV, 2588 eV and 2748 eV corresponding to ions backscattered by O, Al, Ag and Au, respectively. Fig. 8 is focused on the peak related to Ag and Au on co-precipitated Au–Ag/Al and Ag/AuAl obtained from sequential deposition recorded in the same above-mentioned conditions. Regarding the fresh samples in Figs. 8(a) and (b), one can observe the same trends with a surface silver enriched Au–Ag/Al catalyst. Semi-quantitative analysis shows a surface coverage Al/O ratio ~ 0.55. The surface coverage of Au and Ag, of, respectively, 0.33 and 1.13, leads to a Au/Ag ratio ~ 0.29. Further comparisons with the bulk composition from elemental analysis (Au/Ag = 0.42) do not highlight significant divergences. All those observations seem to support a preferential formation of intermetallic Au–Ag particles in co-precipitated AuAg/Al catalyst in agreement with UV–visible and ToF-SIMS analysis emphasizing the fact that gold and silver would be quasi-homogeneously distributed from the core to the surface of those bimetallic particles. On the other hand, a different configuration characterizes Au/AgAl and Ag/AuAl catalysts which exhibit a sharp silver-enriched surface compared to the bulk composition.

Table 3
Relative abundance of positive and negative fragments analysed from Tof-SIMS analysis of bimetallic Au–Ag/Al_2O_3 catalysts prepared by sequential deposition Ag/AuAl and co-precipitation Au–Ag/Al.

Fragment	Ag–Au/Al (%)		Au/AgAl (%)	
	Calcined	Used	Calcined	Used
$AgAuCl^-$	0.11	0.13	–	–
$AgAu^-$	0.03	0.03	–	–
$AgAu_2^-$	0.04	0.03	–	–
Au^-	0.15	0.16	0.12	0.10
Au_2^-	0.02	0.01	–	–
Au_3^-	0.04	0.03	–	–
$AgCl_2^-$	–	–	1.75	0.12
$Ag_2Cl_3^-$	–	–	1.66	0.13
$Ag_3Cl_4^-$	–	–	0.52	–
Ag^+	3.09	4.47	1.61	1.92
Ag_2^+	0.24	0.33	–	0.31
Ag_2Cl^+	–	–	0.86	0.20
Ag_3^+	0.62	0.59	–	0.22
$Ag_3O_2^+$	0.22	0.27	–	0.21
$Ag_3Cl_2^+$	–	–	0.54	0.65
Ag_2Au^+	0.13	0.12	–	–
$Ag_4Cl_3^+$	–	–	0.08	–
Ag_5^+	0.08	0.04	–	0.09

3.2.2. *Evolution of the structural and surface properties in the course of the reaction*

N_2 physisorption isotherms reported in Figs. S2–S4 and textural parameters collected in Table 1 do not reveal significant changes in textural properties on aged samples irrespective of the preparation method for gold and silver deposition. The hysteresis is characteristic of mesoporous materials. No significant change on pore size distribution, pore volume and specific surface area (S_{BET}) seems to occur on aged catalysts which emphasizes the relative thermal stability of the textural properties of those solids in our operating conditions (500 °C in wet atmosphere 10 vol.% H_2O).

Table 2
Surface analysis of fresh and aged bimetallic Au–Ag/Al_2O_3 catalysts after TPR-2 experiments.

Catalyst		Bulk composition		B.E. values (eV)[a]		Surface	Atomic	Composition
		Ag (wt.%)	Au(wt.%)	Au $4f_{7/2}$	Ag $3d_{5/2}$	Au (%)[b]	Ag (%)[b]	Au/Ag
Au–Ag/Al	Fresh	0.98	0.90	84.0	368.2	0.37	0.68	0.54
	Aged[c]			84.0	368.2	0.30	0.80	0.38
Ag/AuAl	Fresh	1.04	0.80	84.3	368.3	<0.1	0.14	0.071
	Aged[c]			84.3	368.6	<0.1	0.27	n.m.
Au/AgAl	Fresh	1.01	0.60	84.1	368.5	<0.1	0.24	0.041
	Aged[c]			84.0	368.4	<0.1	0.21	0.048

[a] Binding energy (BE) expressed in eV (accuracy ± 0.1 eV).
[b] Surface atomic composition (relative accuracy ± 10–20%).
[c] pre-reduced in pure H_2 at 250 °C and exposed overnight at 500 °C to 300 ppm NO, 300 ppm CO, 300 ppm propene, 100 ppm decane, 0.2 vol. % H_2, 5 vol.% H_2O, 10 vol.% CO_2, 10 vol.% O_2.

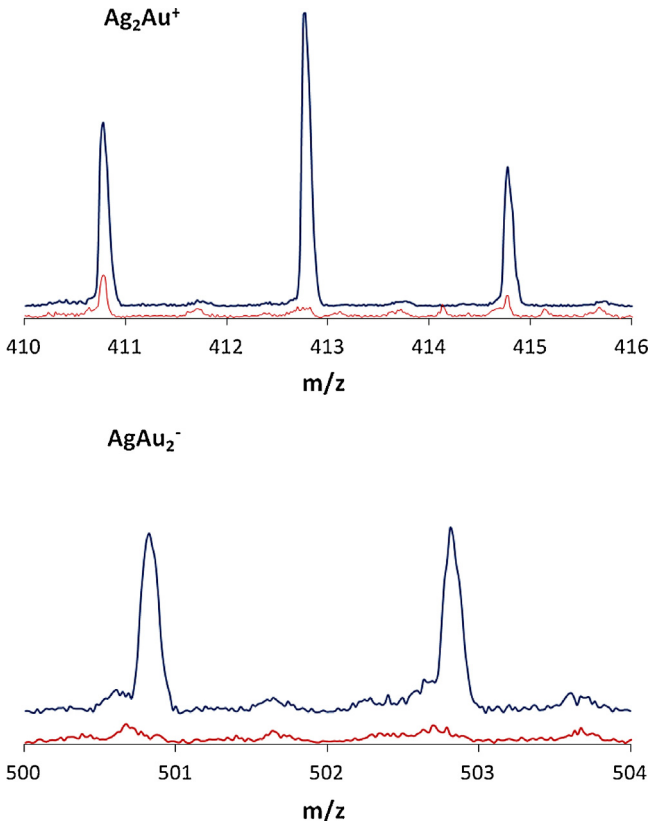

Fig. 6. ToF-SIMS analysis of freshly-prepared Au–Ag/Al_2O_3 prepared by co-precipitation (blue) and sequential deposition (red)—relative abundance of *m/z* signal corresponding to Ag_2Au^+ and $AgAu_2^-$ in positive and negative polarization. (For interpretation of the references to color in this figure legend, the reader is referred to the web version of this article.)

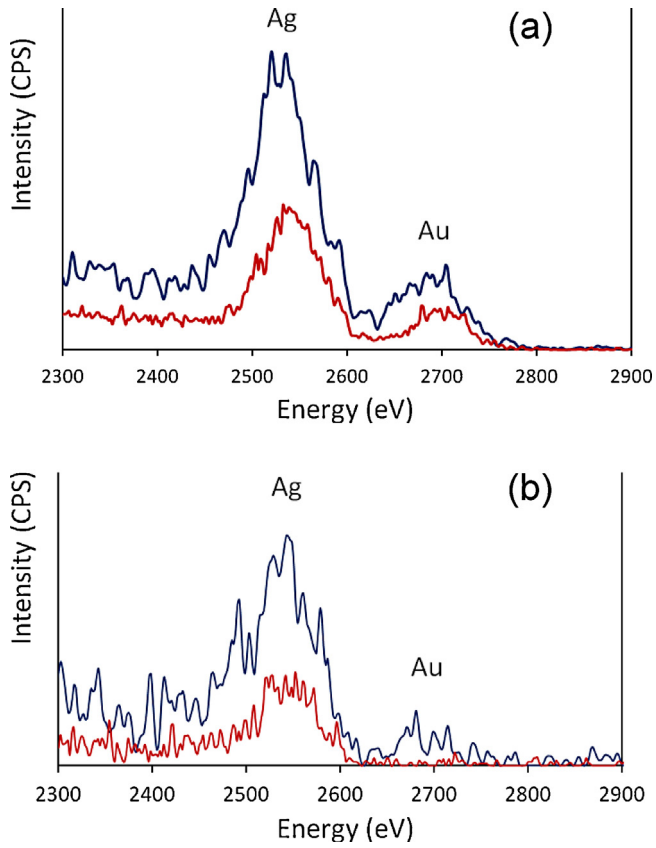

Fig. 8. LEIS spectrum performed with 3 keV $^4He^+$ scattering on freshly-prepared (blue) and aged samples (red) after reaction overnight at 500 °C: (a) Au–Ag/Al and (b)Ag/AuAl. (For interpretation of the references to color in this figure legend, the reader is referred to the web version of this article.)

Now regarding the stability of nano-sized gold and silver particles after reaction at 500 °C significant surface reconstructions occurred altering differently the bimetallic catalysts. TEM images and particle size distribution are reported in Fig. 9 on pre-reduced Ag/AuAl, Au/AgAl and co-precipitated Au–Ag/Al. One can observe the presence of silver and gold particles of different sizes ranging from 1 to 70 nm but with different distribution according to the preparation methods. Hence, a two-step route leads to the segregation of smaller particles with diameter size in the range 1–10 nm, co-existing with larger ones up to 50 nm, compared to the co-precipitated sample. EDS analysis showed that large particles are essentially composed of Ag whereas smaller gold particles segregate at the surface (results not shown). Such tendency seems more accentuated on Au/AgAl for which small particles in the range 1–10 nm predominantly form. For the co-precipitated sample, larger particles segregate with particle size in the range 11–30 nm. It is obvious that particle sintering during reaction at 500 °C overnight is more accentuated on this sample since most of the particles having size diameter in the range 1–30 nm are converted into larger ones exhibiting diameter up to 100 nm. Interestingly, the reverse tendency seems to occur on Ag/AuAl with the occurrence of re-dispersion processes based on the observation that Au and Ag particles are mostly distributed in the range 1–20 nm. Such a tendency is also verified on the Au/AgAl sample even if this re-dispersion seems less pronounced considering the lower number of particles taken into account for this sample. UV–visible spectroscopy does not reveal drastic changes in spectral features except the shift of low wavelength contribution to lower values (see Fig. 5) which could suggest silver cluster re-dispersion to isolated Ag^+ species. As a matter of fact, ToF-SIMS analysis likely provides information which seems consistent with this latter observation. Indeed, the examination of Table 3 show that the relative intensity of the different fragments coming from the ToF-SIMS analysis of the aged Au/AgAl remains unchanged except when Ag is combined with chlorine. In that case, the relative abundance of $AgCl_2^-$, $Ag_2Cl_3^-$ and Ag_2Cl^+ sharply

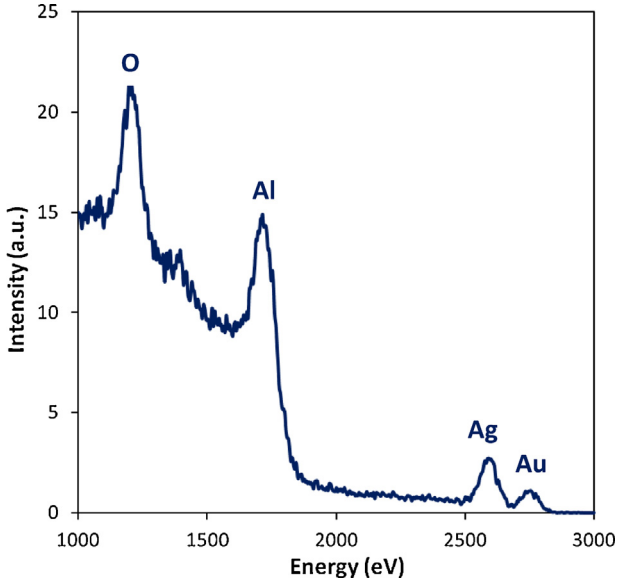

Fig. 7. LEIS spectrum performed with 3 keV $^4He^+$ scattering on co-impregnated Au–Ag/Al samples.

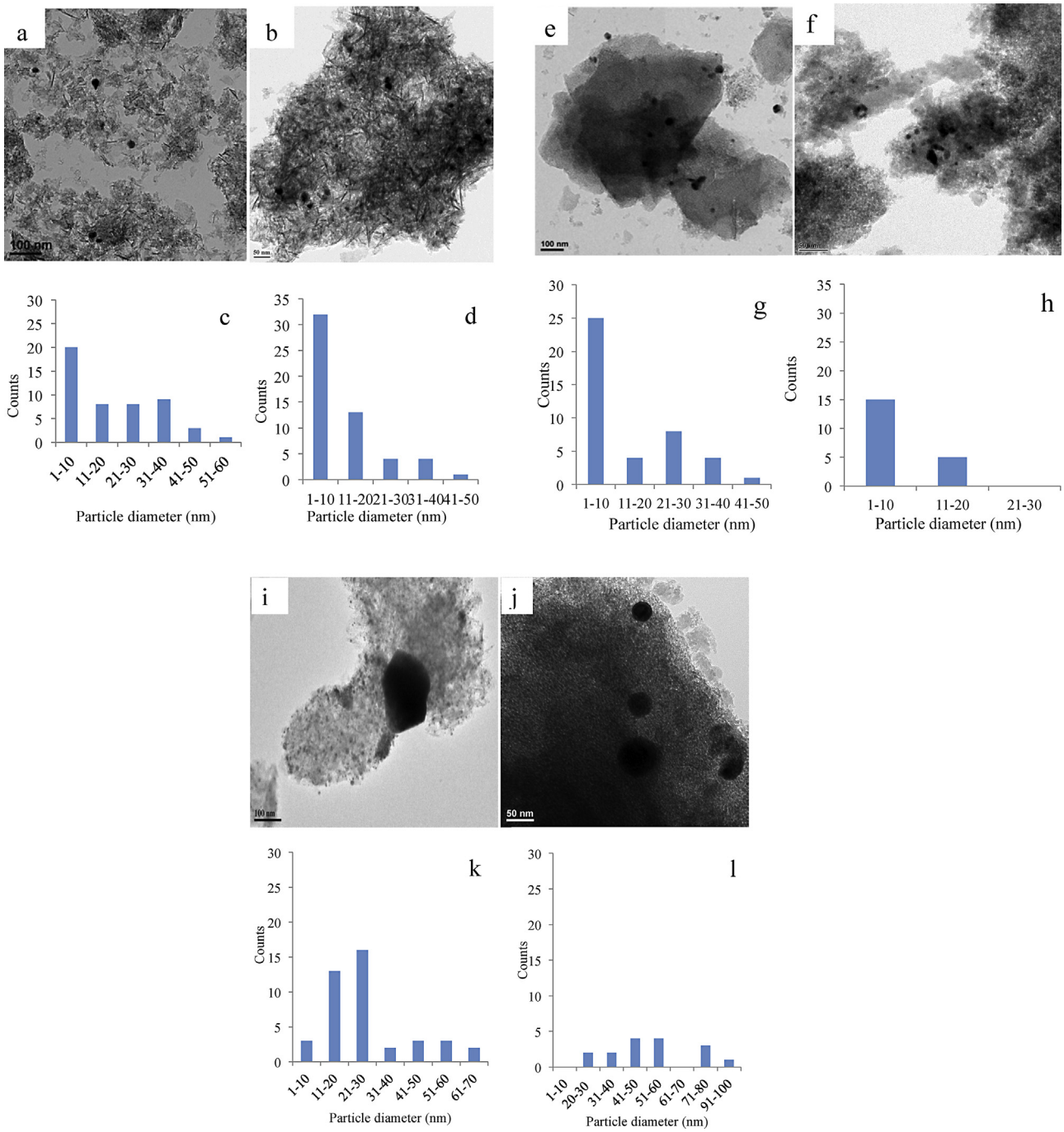

Fig. 9. TEM images and particle size distribution of pretreated catalysts: Ag/AuAl ((a) and (c)), Au/AgAl ((e) and (g)), Ag–Au/Al ((i) and (k)) and aged catalysts Ag/AuAl ((b) and (d)), Au/AgAl ((f) and (h)), Ag–Au/Al ((j) and (l)).

decrease. ToF-SIMS is sensitive to trace amount of chloride coming from the precursor salt of gold ($HAuCl_4$) used during the deposition step. The lowest solubility of AgCl likely originates the formation of large crystallites of AgCl. In our operating conditions, the Deacon reaction taking place above 400 °C under lean atmosphere (with an excess of oxygen) can promote the removal of chlorine. Based on these above-mentioned considerations, Eq. (3) can be envisioned as the starting process for further re-dispersion of silver species.

$$4AgCl_{(s)} + O_{2(g)} = 2Cl_{2(g)} + 2Ag_2O_{(s)} \quad (3)$$

3.3. *Catalytic properties vs. surface properties: How to optimize via a rational method?*

The selective reduction of NO_x under lean conditions involves complex chemical processes at the surface of silver and gold catalysts. It seems obvious that sometimes no consensus can be found regarding the effective role of hydrogen and oxygen depending on the feed gas composition and the nature of intermediates and key elementary steps is still under debate [37,38]. Indeed, the presence or the absence of heavy hydrocarbons, representative of the exhaust gas composition of diesel engines, may also drastically modify the nature of reactions taking place at the catalyst surface,

the nature of intermediates. The structural properties of the surface may be influenced with the equilibration of the oxidation states of silver and gold which likely governs the oxidative/reductive properties of the catalyst. By way of illustration, Arve et al. [37] found a correlation between the complete oxidation of CO and unburnt hydrocarbons (such as hexadecane) to CO_2 and H_2O and a simultaneous increase in the rate of NO conversion to N_2. However, those authors also reported that the rate of the kinetically important steps in HC-SCR partly depends on the chemical nature of the reducing agent (acyclic vs. cyclic hydrocarbons). More recently, different observations have been reported on single gold and silver catalysts supported on alumina associated to an extra production of CO and H_2 [7,34] due to the involvement of reforming and/or partial oxidation of decane. Parallel to that observation, a significant rate enhancement in NO conversion was observed. Up to now, such rate enhancement is not clearly understood and may reflect the bifunctional character of silver and gold based catalysts related to a two-step process involving the intermediate formation of NO_2 as key intermediate in the overall SCR process to N_2. Hence, the presence of metallic and electrophilic gold and silver species on alumina would be needed to catalyze the NO oxidation to NO_2 and the subsequent reduction of NO_2 via the SCR process, respectively [34]. Such behaviour should be likely true over bimetallic Au–Ag catalysts since similar catalytic features can be observed compared to those reported elsewhere [7,34]. The presence of hydrogen in the feed and extra in situ production as suggested in Figs. 1–3 through reforming reaction might be of capital importance to increase the oxidation of NO to NO_2 [39] or to assist the SCR process via the stabilization of nitrates species [38] on the support via the occurrence of spillover processes from the metal to the support. It is also noticeable that the relative rates for these chemical processes are likely intimately related to the structure of the active sites with crystalline metallic silver particles for the NO/O_2 reaction and highly active Ag^+ cations for N_2 production under SCR operating conditions [32] which means a more complex description for bimetallic Au–Ag catalysts taking into account the inhomogeneity in surface composition. Arve et al. [37] pointed out from HRTEM the importance to get 3 nm diameter particles to activate the SCR reactions. However, it seems not the sole parameter to be considered since the balance between Ag^0 and $Ag_n^{\delta+}$ species may drive the selectivity of the reaction which was previously found insensitive to the particle size [34]. Based on the above-mentioned statements, the difficulty to understand surface processes for further optimization of single Au- and Ag-based catalysts is likely related to the versatile properties of the surface which can stabilize differently according to the selected preparation methods, the pre-activation thermal treatments and reaction conditions (temperature, chemical nature of the reducing agent and presence of hydrogen in the feed or in situ produced). All these experimental factors could influence, through surface reconstructions, the particle size, the atomic Ag^0 to $Ag_n^{\delta+}$ ratio and the metal/support interface involved in the overall SCR process.

Up to now, significant attention was not paid to the utilization of bimetallic Au–Ag catalyst for $DeNO_x$ applications. The utilization of these materials is more widespread for oxidative reactions [15,17,32,40–42]. Hence, tuning their oxidative/reductive properties according to the selected method for their preparation is an important outcome. Figs. 1–3 provide important information showing that co-precipitation leads essentially to oxidation reactions, no extra CO formation is observed on the aged sample with a rise in temperature. It is remarkable that a poor activity for NO_x conversion characterizes this catalyst. Subsequent aging overnight at 500 °C (Fig. 1b) accentuates this trend with the disappearance of the broad and weak low temperature range for NO conversion. This can be easily explained by a total oxidation of decane, propene, CO and H_2 into CO_2 and H_2O by oxygen which occurs more readily than the SCR process, then no reducing agent will be available for the parallel reduction of NO. All these trends seem in correct agreement with an accentuation of the metallic character of Ag and Au evidenced from XPS analyses with slightly lower B.E. values compared to those recorded on catalysts prepared by a two-step deposition method and likely in connection to a greater sensibility to particle sintering. Contrarily to co-precipitated samples, the activity of pre-reduced bimetallic Au–Ag catalysts prepared by a two-step method in NO_x conversion develops especially after aging overnight in the reaction mixture at 500 °C (in an excess of oxygen) could be ascribed in a first approximation to an equilibration of the oxidation state of Au and/or Ag starting with a pre-reduced $Au–Ag/Al_2O_3$ catalyst. These samples differ from their surface composition with a systematic surface silver enrichment which could be explained by a greater affinity of Ag to oxygen adsorption than gold and a higher mobility of oxidic silver species [43]. Hence, a first issue of this paper was to relate the different catalytic properties of $Au–Ag/Al_2O_3$ prepared by sequential deposition and co-precipitation to their peculiar surface properties. Second, up to now there is no observation of rate enhancement in NO conversion reported in the literature on modified silver-based catalysts as exemplified in Figs. 2 and 3 on aged $Au–Ag/Al_2O_3$ samples. Recent investigations on single gold catalysts report such observations but in lower extent and at much higher temperature [32]. Hence, an important issue was to describe straightforwardly the different surface reconstructions taking place on the bimetallic samples depending on the protocol used for gold and silver deposition and to correlate this information to a bifunctional catalysis involving a two-step process with initial NO oxidation to NO_2 and then the SCR process [38]. As mentioned above previous investigations emphasized the fact that particle size and shape is not trivial to explain the kinetics and activity of silver based catalysts. However, in the case of bimetallic catalysts, the surface composition should be considered and would depend on the type of interactions between Au and Ag.

Regarding the impact of intermetallic effects or segregation in case of bimetallic particles, it was previously reported for the CO/O_2 reaction that their behaviour is drastically different. This is particularly true for CO oxidation at low temperature with small gold particles (2–5 nm) generally considered as the most active while larger ones become inactive. On the other hand, Au–Ag particles with particle sizes in the range 20–50 nm after pre-reduction in H_2 at 550–650 °C become exceptionally active [41]. Returning to our observations, they do not allow to state on possible particle size dependency of the rate of NO conversion. This can be consistent with previous observations related to the low particle size dependency of the $Ag^0/Ag_n^{\delta+}$ ratio [34]. The most prominent observation is related to a promotional effect of re-dispersion process on the activity taking place at 500 °C under reactive conditions. Hence, both particle size and inhomogeneity in surface composition are probably responsible of the gain in activity. Indeed, DRS analysis of aged Ag/AuAl reveals that cationic Ag species are still detected after reaction at 500 °C suggesting the preservation of Ag+ and $Ag_n^{\delta+}$ clusters and no significant strengthening of the metallic character compared to previous observations on co-impregnated sample due to thermal sintering. On the other hand, the shift observed on the characteristic UV–visible absorption band of Ag^+ compared to ToF-SIMS analysis, shows that the nature and the distribution of Ag^+ species would drastically change on the aged Ag/AuAl catalyst. Indeed, instead of large particles ascribed to the aggregation of AgCl [44] significant re-dispersion would occur through reaction described in Eq. (3) possibly into Ag_2O and or Ag^0 clusters. Changes in spectral features observed on Ag/AuAl could be related to Ag_2O decorating gold particles as earlier proposed for explaining the drastic rate enhancement of large bimetallic having particle in the CO/O_2 reaction. This type of configuration has been already envisioned where Au particles would be decorated by a discontinuous

surface oxide layer [45]. Ag_2O would strongly interact with gold particles preventing their agglomeration/aggregation and preserving low-coordinated Au atoms interacting with AgO_x patches [46]. While such an explanation could be valid, it cannot completely rationalized results obtained from LEIS analysis showing a preferential Ag enrichment of the outermost surface. Such an observation could be consistent with the formation of core–shell structures with surface Ag enriched Au–Ag particles on Ag/AuAl with a core mainly composed of gold. This configuration could be still in agreement with the explanation provided by Wang et al. [45] involving a close interaction between metallic and electrophilic Ag sites for the activation of the NO reduction to nitrogen. This explanation seems consistent with earlier investigation reporting that Ag^+ can adsorb preferentially onto gold surface rather than onto alumina support on the basis of the strong electrostatic attraction between Au and Ag^+ [45]. Such statement is supported by DFT calculations revealing that gold particles are slightly negatively charged [45].

Hence, the synergistic effect observed of freshly-prepared more accentuated on aged bimetallic catalysts could be related to the creation of active site at the interface of metallic gold or Ag particles and AgO_x patches.

4. Conclusion

The catalytic performances of bimetallic Au–Ag/Al_2O_3 catalysts are sensitive to the preparation protocol. Optimal surface properties involve the participation of metallic and electrophilic sites to catalyse, respectively, NO oxidation to NO_2 and its subsequent reduction to nitrogen. Different parameters can contribute to get such an optimal balance taking into account the size, the shape of the particles and inhomogeneity in surface composition in the case of bimetallic catalysts. It was found that co-precipitation leads to the preferential formation of intermetallic compounds particles more active for oxidative reaction than reductive ones resulting in a poor conversion of NO_x to nitrogen. Subsequent exposure at high temperature in reactive conditions has a strong detrimental effect due to particle sintering altering the metal/support interface and a preservation of the metallic character which favour the total oxidation of reducing agents. For catalysts prepared by a sequential deposition method, starting from Au/Al_2O_3 or Ag/Al_2O_3 and then introducing, respectively, silver or gold leads inevitably to a significant surface silver enrichment. This option leads to a considerable improvement in NO conversion which was ascribed to a synergistic effect between Au and Ag with redispersion processes of large AgCl particles into Ag_2O/Ag^0 interacting with gold particles limiting thermal sintering during aging at 500 °C.

Acknowledgements

PM acknowledges UGC for fellowship and CNRS for their help. Financial support from DST is acknowledged for the project SR/S1/IC-42/2009. Mr. R. Gholap and Mr. Ketan Bhotkar (TEM, EDS) are acknowledged for their support in characterization. This work is carried out under “International Associated Laboratory Programme” between UCCS (CNRS) and NCL (CSIR). The Fonds Européen de Développement Régional (FEDER), CNRS, Région Nord Pas-de-Calais and Ministère de l’Education Nationale de l’Enseignement Supérieur et de la Recherche are acknowledged for fundings of XPS/LEIS/ToF-SIMS spectrometers within the Pôle Régional d’Analyses de Surface. The TEM facility in Lille (France) is supported by the Conseil Regional du Nord-Pas de Calais, and the European Regional Development Fund (ERDF).

Appendix A. Supplementary data

Supplementary data associated with this article can be found, in the online version, at http://dx.doi.org/10.1016/j.apcatb.2014.06.031.

References

[1] M. Iwamoto, H. Yahiro, Catal. Today 22 (1994) 5–18.
[2] M. Koebel, M. Elsener, M. Kleemann, Catal. Today 59 (2000) 335–345.
[3] J. Oh, K. Lee, Fuel 119 (2014) 90–97.
[4] F. Birkhold, U. Meingast, P. Wassermann, O. Deutschmann, Appl. Catal., B: Environ. 70 (31) (2007) 119–127.
[5] J.A. Sullivan, O. Keane, Appl. Catal., B: Environ. 70 (2007) 205–214.
[6] M. Colombo, I. Nova, E. Tronconi, V. Schmeißer, B. Bandl-Konrad, L. Zimmermann, Appl. Catal., B: Environ. 142–143 (2013) 861–876.
[7] (a) D.L. Nguyen, S.B. Umbarkar, M.K. Dongare, C. Lancelot, J.S. Girardon, C. Dujardin, P. Granger, Catal. Comm. 26 (2012) 225–230;
(b) D.L. Nguyen, S.B. Umbarkar, M.K. Dongare, C. Lancelot, J.S. Girardon, C. Dujardin, P. Granger, Top. Catal. 56 (2013) 157–164.
[8] N. Jagtap, S.B. Umbarkar, P. Miquel, P. Granger, M. Dongare, Appl. Catal., B: Environ. 90 (2009) 416–425.
[9] B. Wichterlová, P. Sazama, J.P. Breen, R. Burch, C.J. Hill, L. Čapek, Z. Sobalík, J. Catal. 235 (2005) 195–200.
[10] A. Ueda, T. Oshima, M. Haruta, Appl. Catal., B: Environ. 12 (1997) 81–93.
[11] K. Arve, O. Adam, L. Simakova, K. Capek, D. Eranen, Yu. Murzin, Top. Catal. 52 (2009) 1762–1765.
[12] P. Miquel, P. Granger, N. Jagtap, S. Umbarkar, M. Dongare, C. Dujardin, J. Mol. Catal. A: Chem. 322 (2010) 90–97.
[13] J.P. Breen, R. Burch, C. Hardacre, C.J. Hill, B. Krutzsch, B. Bandl-Konrad, E. Jobson, L. Cider, P.G. Blakeman, L.J. Peace, M.V. Twigg, M. Preis, M. Gottschling, Appl. Catal., B: Environ. 70 (2007) 36–44.
[14] A. Ueda, M. Aruta, Appl. Catal., B: Environ. 18 (1998) 115–121.
[15] C. Hamill, R. Burch, A. Goguet, D. Rooney, H. Driss, L. Petrov, M. Daous, Appl. Catal., B: Environ. 147 (2014) 864–870.
[16] X. Liu, A. Wang, X. Yang, T. Zhang, C.-Y. Mou, D.-S. Su, J. Li, Chem. Mater. 21 (2009) 410–418.
[17] X. Liu, A. Wang, X. Wang, C.-Y. Mou, T. Zhang, Chem. Commun. (2008) 3187–3189.
[18] X.Y. Liu, A.Q. Wang, L. Li, T. Zhang, C.Y. Mou, J.F. Lee, J. Catal. 278 (2011) 288–296.
[19] A. Sandoval, A. Aguilar, C. Louis, A. Traverse, R. Zanella, J. Catal. 281 (2011) 40–49.
[20] Z. Qu, G. Ke, Y. Wang, M. Liu, T. Jiang, J. Gao, Appl. Surf. Sci. 277 (2013) 293–301.
[21] A.-Q. Wang, J.-H. Liu, S.D. Lin, T.-S. Lin, C.-Y. Mou, J. Catal. 233 (2005) 186–197.
[22] D.A. Shirley, Phys. Rev. B: Condens. Matter 5 (12) (1972) 4709–4714.
[23] H.H. Brongersma, T. Grehl, P.A. van Hal, N.C.W. Kuijpers, S.G.J. Mathijssen, E.R. Schofield, R.A.P. Smith, H.R.J. ter Veen, Vacuum 84 (2010) 1005–1007.
[24] K. Eranen, F. Klingsted, K. Arve, L.E. Lindfors, D.Y. Murzin, J. Catal. 227 (2004) 328–343.
[25] R. Burch, T.C. Watling, J. Catal. 169 (1997) 45–54.
[26] D.Y. Yoon, J.H. Park, H.C. Kang, P.S. Kim, I.S. Nam, G.K. Yeo, J.K. Kil, M.S. Cha, Appl. Catal., B: Environ. 101 (2011) 275–282.
[27] T. Déronzier, F. Morfin, M. Lomello, J.L. Rousset, J. Catal. 311 (2014) 221–229.
[28] J. Zheng, H. Lin, Y.N. Wang, X. Zheng, X. Duan, Y. Yuan, J. Catal. 297 (2013) 110–118.
[29] X. Bokhimi, R. Zanella, V. Maturano, A. Morales, Mater. Chem. Phys. 138 (2013) 490–499.
[30] C.A. Foss, G.L. Hornyak, J.A. Stockert, C.R. Martin, J. Phys. Chem. 98 (1994) 2963–2971.
[31] B.M.I. van der Zande, M.R. Bohmer, L.G.J. Fokkink, C.J. Schnenberger, J. Phys. Chem. B 101 (1997) 852–854.
[32] N. Bogdanchikova, F.C. Meunier, M. Avalos-Borja, J.P. Breen, A. Pestryakov, Appl. Catal., B: Environ. 36 (2002) 287–297.
[33] L. Zhang, C. Wang, Y. Zhang, Appl. Surf. Sci. 258 (2012) 5312–5318.
[34] V.I. Parvulescu, B. Cojocaru, V. Parvulescu, R. Richards, Z. Li, C. Cadigan, P. Granger, P. Miquel, C. Hardacre, J. Catal. 272 (2010) 92–100.
[35] W.L. Dai, Y. Cao, L.P. Ren, X.L. Yang, J.H. Xu, H.X. Li, H.Y. He, K.N. Fan, J. Catal. 228 (2004) 80–91.
[36] L.-T. Weng, Appl. Catal., A: Gen. 474 (2014) 203–210.
[37] K. Arve, J.R. Hernandez Carucci, K. Eränen, A. Aho, D.Y. Murzin, Appl. Catal., B: Environ. 90 (2009) 603–612.
[38] S. Tamm, N. Vallim, M. Skoglundh, L. Olsson, J. Catal. 307 (2013) 153–161.
[39] S. Tamm, S. Fogel, P. Gabrielsson, M. Skoglundh, L. Olsson, Appl. Catal., B: Environ. 136–137 (2013) 168–176.
[40] H. Zhang, N. Toshima, Appl. Catal., A: Gen. 447–448 (2012) 81–88.
[41] X. Huang, X. Wang, X. Wang, X. Wang, M. Tuan, W. Ding, X. Lu, J. Catal. 301 (2013) 217–226.
[42] X. Liu, Y. Li, J.W. Lee, C?Y. Hong, C.Y. Mou, B.W.L. Jang, Appl. Catal., A: Gen. 439–440 (2012) 8–14.
[43] N. Toreis, X.E. Verykios, S.M. Khalid, G.B. Bunker, Surf. Sci. 197 (1988) 415–429.
[44] A.Q. Wang, Y. Hsieh, Y.F. Chen, C.Y. Mou, J. Catal. 237 (2006) 197–206.
[45] A. Wang, X.Y. Liu, C.-Y. Mou, T. Zhang, J. Catal. 308 (2013) 258–271.
[46] J.H. Liu, A.Q. Wang, Y.S. Chi, H.P. Lin, C.-Y. Mou, D.S. Su, J. Phys. Chem. B 109 (2005) 40–43.